Journal of
Composites Science

MDPI

Article

Enhanced X-ray Visibility of Shape Memory Polymer Foam Using Iodine Motifs and Tantalum Microparticles

Lindy K. Jang [1], Landon D. Nash [2], Grace K. Fletcher [1], Thomas Cheung [1], Andrew Soewito [1] and Duncan J. Maitland [1,2,*]

[1] Department of Biomedical Engineering, Texas A&M University, College Station, TX 77843, USA; lindy7@tamu.edu (L.K.J.); gracekfletch@tamu.edu (G.K.F.); thomasbc132@tamu.edu (T.C.); asoewito@tamu.edu (A.S.)
[2] Shape Memory Medical, 807 Aldo Ave., Santa Clara, CA 95054, USA; landon@shapemem.com
* Correspondence: djmaitland@tamu.edu

Abstract: Shape memory polymer (SMP) foams are porous materials with high surface area and large volumetric expansion capabilities that are well suited for endovascular occlusion applications, including brain aneurysm embolization. However, many polyurethane SMP foams are inherently radiolucent when X-ray visibility is required to ensure the safe delivery of the foam to the targeted aneurysm site using fluoroscopy. Here, highly radio-dense tantalum microparticles were added to a previously reported triiodobenzene-containing SMP foam (ATIPA foam) premix to fabricate ATIPA foam-tantalum composites (AT_T). The AT_T foams showed comparable glass transition temperatures, faster expansion profiles, increased X-ray visibility, good cytocompatibility, and faster oxidative degradation compared to the control ATIPA foam without tantalum. The mechanical properties were improved up to 4 vol% tantalum and the X-ray visibility was most appropriate for the 2 vol% (AT_2%T) and 4 vol% (AT_4%T) tantalum foams. E-beam sterilization did not impair the critical properties of the ATIPA foams. Overall, AT_2%T was the optimal foam composition for neurovascular prototypes due to its high oxidative stability in vitro compared to previous low-density SMP foams. The AT_T foams are very promising materials with high toughness and sufficient X-ray visibility for use as neurovascular embolization devices.

Keywords: shape memory polymer foam; X-ray visibility; tantalum microparticles; neurovascular embolization device; intracranial aneurysm

Citation: Jang, L.K.; Nash, L.D.; Fletcher, G.K.; Cheung, T.; Soewito, A.; Maitland, D.J. Enhanced X-ray Visibility of Shape Memory Polymer Foam Using Iodine Motifs and Tantalum Microparticles. *J. Compos. Sci.* **2021**, *5*, 14. https://doi.org/10.3390/jcs5010014

Received: 22 December 2020
Accepted: 3 January 2021
Published: 6 January 2021

1. Introduction

Intracranial aneurysms are localized pathological dilations of cerebral arteries that occur in approximately 4% of the population [1]. Approximately 90% of intracranial aneurysms are saccular aneurysms, which are commonly formed at arterial bifurcations of the circle of Willis [2]. In the United States, approximately 30,000 people suffer from rupture of aneurysm annually, which leads to subarachnoid hemorrhage (SAH). SAH has a high case-fatality rate of 25–50% caused by an initial bleed or immediate complications, and half of the survivors have permanent neurological damage [3,4]. Since the development of detachable coiling using a microcatheter in 1990, endovascular treatment has been the standard treatment method for intracranial aneurysms, substituting invasive craniotomies necessary for surgical clipping [5]. However, recanalization is a major problem that occurs in up to 25% of aneurysms treated with platinum coils, especially in wide-neck or large-to-giant aneurysms [6,7]. One of the most significant contributing factors of aneurysm recurrence is coil compaction, which is caused by the water-hammer effect of pulsatile blood flow [8]. To prevent coil compaction, increasing the packing density of an embolization device is critical. However, it is not usually achievable in wide-neck aneurysms or large aneurysms with volumes larger than 600 mm^3 [9].

Polyurethane shape memory polymer (SMP) foams have shown great promise in endovascular embolization devices due to long-term biocompatibility, rapid thrombosis, and unique shape recovery capabilities [10–13]. SMP foams are soft and open-celled porous materials that can be crimped into a secondary shape and maintain the shape until actuated by a thermal stimulus to recover their original shape. This allows a low-volumetric SMP foam to be delivered to the desired spot (e.g., aneurysm sac) using a microcatheter where the foam can expand to its porous primary shape when actuated by body temperature or an external heat stimulus. SMP foams have interconnected pores that allow blood to flow inside the scaffold and form interconnected thrombus, promoting subsequent cell infiltration that triggers the tissue healing process in the matrix [13,14]. SMP foam-coated coils showed a bulk packing density of 93% in an in vitro wide-neck aneurysm, which was significantly higher than previously reported packing densities of bare platinum coils (BPC; 30–31%) or hydrogel coated coils (76–85%) [12]. In vivo studies in porcine sidewall aneurysm models demonstrated connective tissue formation in the SMP foam-treated aneurysms and neointima layer formation over the neck of the treated aneurysms [14,15]. SMP foam-treated aneurysms have shown more mature connective tissue, thicker fibrous cap across the aneurysm neck, and more rapid healing compared to coil-treated porcine vein pouch aneurysms [15]. SMP foam material was also used in a clinical study to embolize a false lumen of a post-dissection aneurysm in a 69-year-old patient, which resulted in complete and stable thrombosis of the false lumen at 15 months [16]. However, SMP foams do not have inherent radiopacity, which limits their clinical utility as endovascular devices since X-ray visualization is necessary for safely delivering the device to the target site, properly packing devices into an aneurysm, and tracking the implant over time.

One approach to circumventing the lack of SMP X-ray visibility is to incorporate high-Z markers into the device design. Kashyap et al. three-dimensionally (3D) printed and salt leached thermoplastic SMP containing tungsten particulates to fabricate radiopaque and porous endovascular embolization material [17]. However, the fabricated SMP had too high density (~1 g/cm^3) and too stiff modulus (~1 GPa) to be used as a neurovascular device. In the case of low-density SMP foams, one of the methods is to use BPCs as a backbone for SMP foams to visualize the foam devices being delivered to the aneurysm sites [11,12]. However, the use of BPC restricts the aneurysm lesion shrinkage when the collagenous connective tissue formed around the device is contracted in the late healing stage, which would delay the overall healing [15]. Hasan et al. physically incorporated tungsten nanoparticles into SMP foams to increase the X-ray visibility. Sufficient radiopacity was achieved at 6 vol% tungsten foams, but the mechanical toughness was diminished significantly [18]. Nash et al. reported chemically modified, triiodobenzene monomer (5-amino-2,4,6-triiodoisophthalic acid; ATIPA)-containing SMP foams with increased X-ray visibility and mechanical toughness. However, the degree of radiopacity was still not sufficient for the neurovascular device scale (2 mm diameter) [19], motivating the need for further opacification.

Tantalum is a good candidate material as an X-ray-visible additive due to its excellent biocompatibility, ductility, corrosion resistance, and radiopacity [20,21]. Tantalum has been in clinical use since 1940 and has shown great in vivo bioactivity, exhibiting abundant cellular adherence, growth, and extracellular matrix formation on tantalum coated surface [20,22]. In this study, tantalum microparticles were loaded in the ATIPA foaming mixtures to further enhance X-ray visibility of the ATIPA SMP foam. In addition, cell opening additives were added during the foaming process to make a more open cell structure, which will prevent the foam from shrinking during curing. Thermal properties, mechanical properties, chemical properties, radiopacity, cytocompatibility, and extractables were characterized. The effect of E-beam sterilization on chemical, thermal, and mechanical properties of tantalum-loaded ATIPA foams (AT_T) was also analyzed, in addition to the in vitro degradation behavior (oxidative and hydrolytic) after E-beam sterilization.

2. Materials and Methods

2.1. Materials

The 5-amino-2,4,6-triiodoisophthalic acid (ATIPA; Sigma Aldrich, St. Louis, MO, USA), 3-methyl-1,5-pentanediol (MPD; Sigma Aldrich), 1,2,6-hexanetriol (HT; Sigma Aldrich), 2-butyl-2-ethyl propanediol (BEP; VWR Scientific, Radnor, PA, USA), hemxamethylene diisocyanate (HDI; TCI America, Portland, OR, USA), Enovate 245fa Blowing Agent (Honeywell International, Houston, TX, USA), tantalum powder (APS~2 µm, 99.9%; Alfa Aesar, Tewksbury, MA), Tegostab B8523 (Evonik, Essen, Germany), 2-propanol 99% (IPA; VWR Scientific), tetrahydrofuran (THF; Millipore, Billerica, MA, USA), Dulbecco's Modified Eagle Medium (DMEM; Sigma Aldrich), and deionized (DI) water (>17 MΩcm purity; Millipore water purifier system; Millipore) were used as received.

2.2. Synthesis of Tantalum-Loaded ATIPA SMP Foam

ATIPA SMP foams with tantalum microparticles (AT_T) were synthesized based on the protocol described by Nash et al. [19]. Hydroxyl (OH) premix was prepared one day before foaming by adding 0.6 equivalent of ATIPA, MPD, BEP, and HT. The OH premix was mixed for 30 s at 3500 rpm using a Flacktek high-speed shear mixer, heated at 50 °C for one hour, mixed for 30 s at 3500 rpm, heated overnight at 50 °C, and mixed for 30 s at 3500 rpm before foaming. Isocyanate (NCO) premix was prepared two days before foaming in a desiccated glove box by adding 0.4 equivalent of ATIPA, MPD, BEP, and HT. The NCO premix was mixed at 3500 rpm for 30 s, heated at 50 °C for an hour, mixed at 3500 rpm for 30 s, and heated at 50 °C overnight. On the next day, 1 equivalent of HDI was added to the NCO premix and it was mixed for 10 min at 3500 rpm and placed on a room temperature shaker overnight at 60 rpm. On the foaming day, the viscosity of NCO premix was checked to be like honey and if it was less viscous, it was shaken for an additional day. An amount of 0, 2, 4, and 8 vol% tantalum powder was added to the NCO premix and mixed for 30 s at 3500 rpm. The mixture of 4 wt% of surfactant DC1990 and 0.025 wt% of Tegostab B8523 was added to the NCO premix and mixed for 30 s at 3500 rpm. The OH premix was added to the NCO premix and mixed for 30 s. After adding 1.5 mL Enovate and mixing for 15 s, the mixture was cured for 20 min at 90 °C. The foam skin was removed by a razor blade and then post-cured at 50 °C overnight. The detailed foam composition is shown in Table 1. All the foam samples were thoroughly cleaned with reverse osmosis (RO) water (30 min, sonicated), IPA (30 min × 4 times, sonicated) and RO water again (15 min × 4 times, sonicated). Foam samples were dried at 50 °C overnight and stored at room temperature under vacuum before use.

Table 1. AT_T SMP foam compositions with varying amounts of tantalum.

Sample Name	ATIPA (eq%)	MPD (eq%)	BEP (eq%)	HT (eq%)	HDI (eq%)	Tantalum (vol%)	Tegostab B8523 (wt%)	Enovate (mL)	Scale (g)
AT	20	40	20	20	100	0	0.025	1.5	8
AT_2%T	20	40	20	20	100	2	0.025	1.5	8
AT_4%T	20	40	20	20	100	4	0.025	1.5	8
AT_8%T	20	40	20	20	100	8	0.025	1.5	8

2.3. Physical and Morphological Characterization

Foam density was calculated by foam mass divided by the foam's bulk volume. Foams were cut into 1 cm^3 cubes and the mass was measured (n = 5).

Pore size was measured using images taken from scanning electron microscopy (SEM; JCM-5000 Neoscope, JEOL, Peabody, MA, USA). For SEM sample preparation, foams were cut into slices with a thickness of 3 mm and sputter coated. Five images were taken for each foam composition. Random 5–6 pores were selected per image and their diameters were measured using ImageJ software (n = 20).

Gel fraction was calculated by the final sample mass divided by the original sample mass. Foam samples were cut into 1 cm^3 cubes. The samples were cleaned three times with IPA (1:20 volume ratio) for 30 min each using sonication to remove any residual surfactants. Then the samples were dried at 100 °C overnight and the mass was recorded. THF (1:20 volume ratio) was added to the samples, heated at 50 °C for 48 h, and dried at 70 °C after removing THF for 36 h. The final mass of the samples was recorded (n = 5).

2.4. ATR-FTIR Spectroscopy

The absorbance of foam samples was measured using attenuated total reflectance Fourier transform infrared (ATR-FTIR) spectroscopy (Bruker ALPHA, diamond ATR crystal, Bruker, Billerica, MA, USA). Bruker OPUS Spectroscopy software was used to analyze the spectra.

2.5. Differential Scanning Calorimetry (DSC)

Glass transition temperatures (T_g) of dry samples (dry T_g) and water-plasticized samples (wet T_g) were analyzed using differential scanning calorimetry (DSC Q200, TA Instruments, New Castle, DE, USA,). For the dry T_g measurement, dry foam samples (2–4 mg, n = 3) were loaded into Tzero pans and two heating cycles were run, of which the second cycle was used to obtain the dry T_g (heating range: −40~120 °C, ramp rate: 10 °C/min, 1 min equilibration at each endpoint). For wet T_g measurement, the dry mass of the samples were measured (2–4 mg, n = 3) and the samples were submerged in 50 °C water for 30 min. Excess water was squeezed out using a laboratory wipe until the water uptake was smaller than 10% of the original sample mass. Samples were loaded into Tzero pans and only one cycle was run to determine the wet T_g (heating range: −40~120 °C, ramp rate: 10 °C/min). Pyris software was used to determine the T_gs of the samples.

2.6. Dynamic Mechanical Analysis (DMA)

Foam samples were punched into cylinders with a diameter of 6 mm and a thickness of 5 mm. Thermomechanical properties of the foams were analyzed using a TA Q800 Dynamic Mechanical Analyzer (TA Instruments, New Castle, DE, USA) with a compression mode. Foams were equilibrated at 20 °C for 5 min and heated to 100 °C at a rate of 3 °C/min, with an amplitude of 40 μm at 1 Hz and a preload of 0.01 N.

2.7. Expansion Study

Foams were punched into cylindrical shapes with a diameter of 2 mm and a length of 1.5 cm (n = 3). The samples were axially threaded over 0.006″ wires. The foam crimper (Machine Solutions SC250) was pre-heated to 100 °C for 15 min. Foams were radially compressed at 100 °C, constrained while cooling to room temperature, and released from the crimper. Crimped foams were placed under vacuum for 24 h before the expansion test. Foams over wires were submerged in 37 °C water and the expanding foams were imaged every one minute until five minutes, and every five minutes until 40 min. Diameters of the expanding foams at five sites along the length were measured using ImageJ software.

2.8. Mechanical Testing

Samples were prepared by cutting them into an ASTM D-638-V dog bone shape. The shorter ends of the dog bone samples were epoxy glued to wooden blocks and they were rested for 24 h for complete cure. The attached wooden blocks were fixed to clamps on MTS Insight 30 Universal Tensile Tester. Strain-to-failure experiments were performed on the foam samples (n = 5), with a rate of 5 mm/min at room temperature.

2.9. X-ray Spectroscopy

Samples were cut into 1.5 cm × 1.5 cm squares with thicknesses of 8, 4, 2, and 1 mm. Neurovascular-scale foams which were expanded and crimped cylindrical samples with a diameter of 2 mm were prepared. All the foam samples were taped on a plastic tray

as well as two bare platinum coils as positive controls (0.008″ OD 90/10 Pt/Ir coil and 0.008″ OD 92/8 Pt/W coil). X-ray images of the plastic tray containing all the samples were taken using OrthoScan C-arm system (Mobile DI Model 1000-0005). X-ray images were obtained with and without an 0.5″ aluminum plate over the sample tray which was used as a skull analog that attenuates X-rays and imitates the clinical setting of endovascular treatment [23]. Grayscale values were measured on the background of an 8 bit X-ray image and on the samples using ImageJ software. The background value was subtracted from the sample's mean grey scale value.

2.10. Cytocompatibility Test

Extraction media tests were performed on the ATIPA foams with a 3 cm^2/mL extraction ratio according to ISO10993-5. Cell culture media consisted of DMEM, 10% newborn calf serum, 1% penicillin/streptomycin, and 0.1% fungizone. The extracts of each specimen were obtained by submerging discs, with a diameter of 5 mm and a thickness of 2 mm, cut by biopsy punch into 2 mL of media solution. The size of the discs was chosen through consideration of the pore sizes and volume to represent the accessible surface area. The samples were then placed on a shaking incubator for 72 h at 37 °C. Three replicate extraction media samples were made for each foam.

NIH/3T3 mouse fibroblast cells were seeded at an initial 7500 cells per well onto 96-well polystyrene plates and cultured for 24 h at 37 °C and 5% CO_2 in an incubator before treatment with extract media samples. At 24 h, 200 µL of extraction media was used for each well. Cell viability was evaluated using a resazurin assay to quantify metabolic activity 48 h after the addition of extraction media. Resazurin solution was added to cell culture media for a 5% final concentration. Cells were then incubated in the media and resazurin solution for 3 h, where the increase in absorbance at 590 nm relative to a blank (media and 5% resazurin without cells) was measured using a plate reader (Tecan Infinite M200 Pro, Männedorf, Switzerland). The absorbance values for the extract media samples were compared to a negative control (media and 5% resazurin with cells and without extract media) as a percentage, with the negative control representing 100% cell viability.

2.11. E-Beam Sterilization

Samples were packaged in foil film bags (Beacon Converters, Saddle Brook, NJ, USA) with humidity indicators. The packages were vacuum sealed with heat after purging with nitrogen gas using an AVN packaging system (AmeriVacS, San Diego, CA, USA). The sealed packages were E-beam-sterilized at 43.6 kGy E-beam dose (10 MeV, 18 kW) at the National Center for Electron Beam Research (College Station, TX, USA). Alanine films (Kodak, Rochester, NY, USA) were used to measure the actual dose of E-beam using a Bruker E-scan spectrometer (Bruker, Billerica, MA, USA).

2.12. Degradation Analysis

In vitro degradability of foam samples was analyzed in an accelerated oxidative condition (20% H_2O_2) and an accelerated hydrolytic condition (0.1 N NaOH). Samples were prepared by cutting foams into 1 cm^3 cubes (n = 3) and the initial sample mass was recorded. Samples were submerged in 20% H_2O_2 or 0.1 N NaOH with a 1:20 volume ratio (foam:solution) and stored at 37 °C. Degradation solutions were exchanged with fresh solutions every three days to ensure stable pH or ion concentration. The mass change of the samples was recorded every six days. Samples were washed with RO water and ethanol (1:20 volume ratio) and dried at 50 °C under vacuum overnight. The mass of the samples were recorded and the samples were put into fresh degradation solutions. To analyze the chemical and morphological changes of the sample foams over degradation time, ATR-FTIR and SEM analysis were performed every 18 days of degradation.

2.13. Tantalum Extraction Analysis

The AT_2%T was chosen for the extractables study due to its optimal radiopacity and the oxidative stability. The extraction was performed under exaggerated extraction conditions. Foam samples were prepared in neurovascular device scale (2 mm diameter, 1 cm length), and submerged in 5 mL of water (polar extraction) and hexane (non-polar extraction) at 50 °C for 72 h.

To study the effect of the oxidative and hydrolytic degradation solutions on the extraction of tantalum particles from the foam samples, AT_2%T was submerged in 5 mL of 20% H_2O_2 and 0.1 N NaOH at 37 °C for 72 h.

Foam samples were removed from the four extraction solutions. After gently mixing the solutions, 1 mL aliquot was taken and 0.1 mL of concentrated hydrofluoric acid (HF) was added for complete dissolution of tantalum. The aliquot equilibrated for a minimum of one hour in a polypropylene acid digestion tube. For the hexane extraction solution, hexane was evaporated using nitrogen evaporation. Then deionized water was added to the samples to a final volume of 10 mL. A method blank and lab control spike solutions were prepared and got the same treatment as the samples. The samples were analyzed by inductively coupled plasma-optical emission spectrometry (ICP-OES) to determine the amount of tantalum in the extraction solutions. The ICP-OES analysis including the HF treatment was performed at Legend Technical Services Inc. The total amount of tantalum extracted from the neurovascular device was calculated by multiplying the result by the volume of the remaining solutions accounting for the evaporated solvents in the extraction solutions.

3. Results

3.1. Physical Properties of ATIPA-Tantalum Composite (AT_T) Foams

Foam densities of AT_T foams were in the range of 0.045–0.2 g/cm^3 (Figure 1a). AT_T foams showed increasing foam densities as the tantalum content increased. As more tantalum was added to the NCO premix, the foaming mixture became more viscous which led to the lower rising height of the foam and thus, higher density and smaller pore size (Figure 1b). The foaming mixture was especially viscous for AT_8%T after loading 8 vol% tantalum that its final foam height was significantly lower than the other foams, resulting in significantly higher density. A highly viscous foaming mixture could limit the release of gas that was generated inside the bulk foam solution and cause many small pores to form throughout the foam. Furthermore, microparticles serve as nucleation points in foam synthesis due to stress concentration and generate a higher number of pores inside the foam [18]. All of the AT_T foams showed high gel fractions over 90% (Figure 1c). AT foam showed the lowest gel fraction of 92%, whereas AT_2%T, AT_4%T, and AT_8%T foams showed 96% gel fraction. This is attributed to lower density and lower number of nucleation points of AT foam compared to tantalum-added foams.

3.2. Morphological Properties

SEM images in Figure 1d (top) show partially open porous structures of ATIPA foams. The addition of Tegostab B8523, which is a commercial cell opener for polyurethane foams, introduced a higher number of open pores in the foam system compared to the previous ATIPA foam developed by Nash et al. [19]. AT_T foams demonstrated pore sizes ranging from 300 to 1000 µm. AT_8%T showed more homogeneous pore sizes compared to other foams because of the increased nucleation sites and higher density. All of the foams exhibited even distribution of tantalum particles as shown in the smooth surface of the foam membranes and did not show any noticeable agglomerates in the SEM images even at higher magnification (500×).

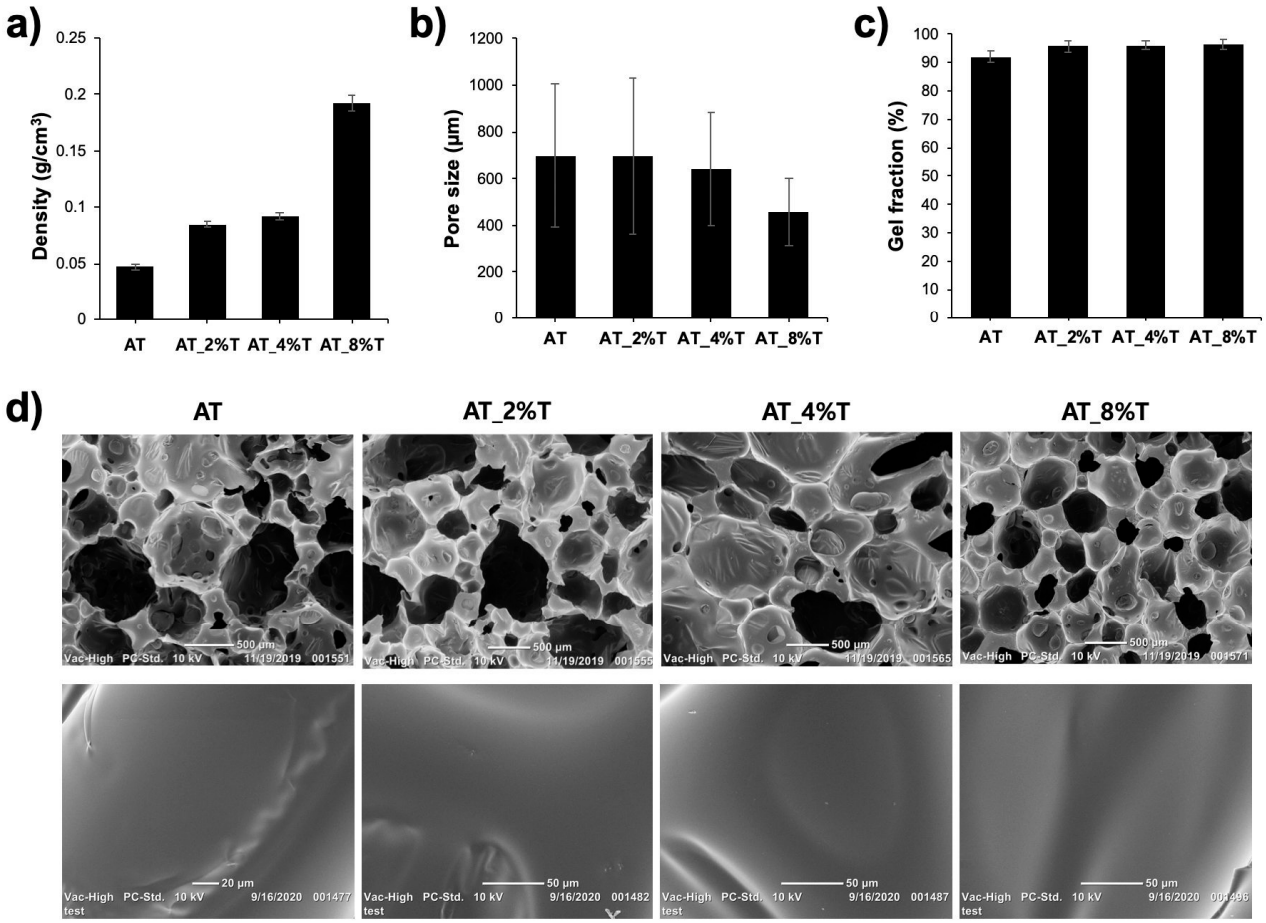

Figure 1. Physical and morphological properties of ATIPA foams. (**a**) Foam densities measured after RO water and IPA cleaning step. (**b**) Pore sizes measured from SEM images using Image J. (**c**) Gel fraction measured after IPA and THF treatment. (**d**) Representative SEM images of the foam morphologies at 30× magnification (top) and 500× magnification (bottom).

3.3. Chemical Characterization

Chemical properties of AT_T foams were analyzed using ATR-FTIR spectroscopy. All of the foams showed identical peaks, indicating that the addition of tantalum microparticles did not change any chemical properties of the control AT foam (Figure 2a). All foams showed a strong hydrogen-bonded urethane C=O peak at 1686 cm^{-1}. This urethane peak was observed in previous polyurethane foams that were made using low-molecular-weight polyols, which is also the case in this study [10]. A urea shoulder peak is present at 1650 cm^{-1}, which is from the urea link formed when the amine group of ATIPA reacted with the isocyanate group of HDI. A broad peak at 3310 cm^{-1} indicates N–H stretching and peaks at 2849 cm^{-1} and 2896 cm^{-1} are from C–H stretching of methyl groups of MPD or BEP. Peaks at 1512 cm^{-1} and 1236 cm^{-1} are from amide II and amide III vibration peaks, respectively, from amide link formed when the carboxylic group of ATIPA reacted with the isocyanate group from HDI.

3.4. Thermal Characterization

Dry T_g and wet T_g of AT_T foams were measured using DSC (Figure 2b). All of the dry T_gs of the foam samples were in the range of 44–47 °C and all of the wet T_gs were in the range of 30–33 °C. There was not any trend observed in between the T_gs of the foam samples, which indicates that the addition of tantalum microparticles did not affect the thermal properties of the foams. Further, dry T_g being higher than 40 °C ensures the safe

storage of the foam devices at dry state at ambient temperature, and wet T_g being lower than 37 °C ensures their ability to expand passively in bloodstreams at body temperature.

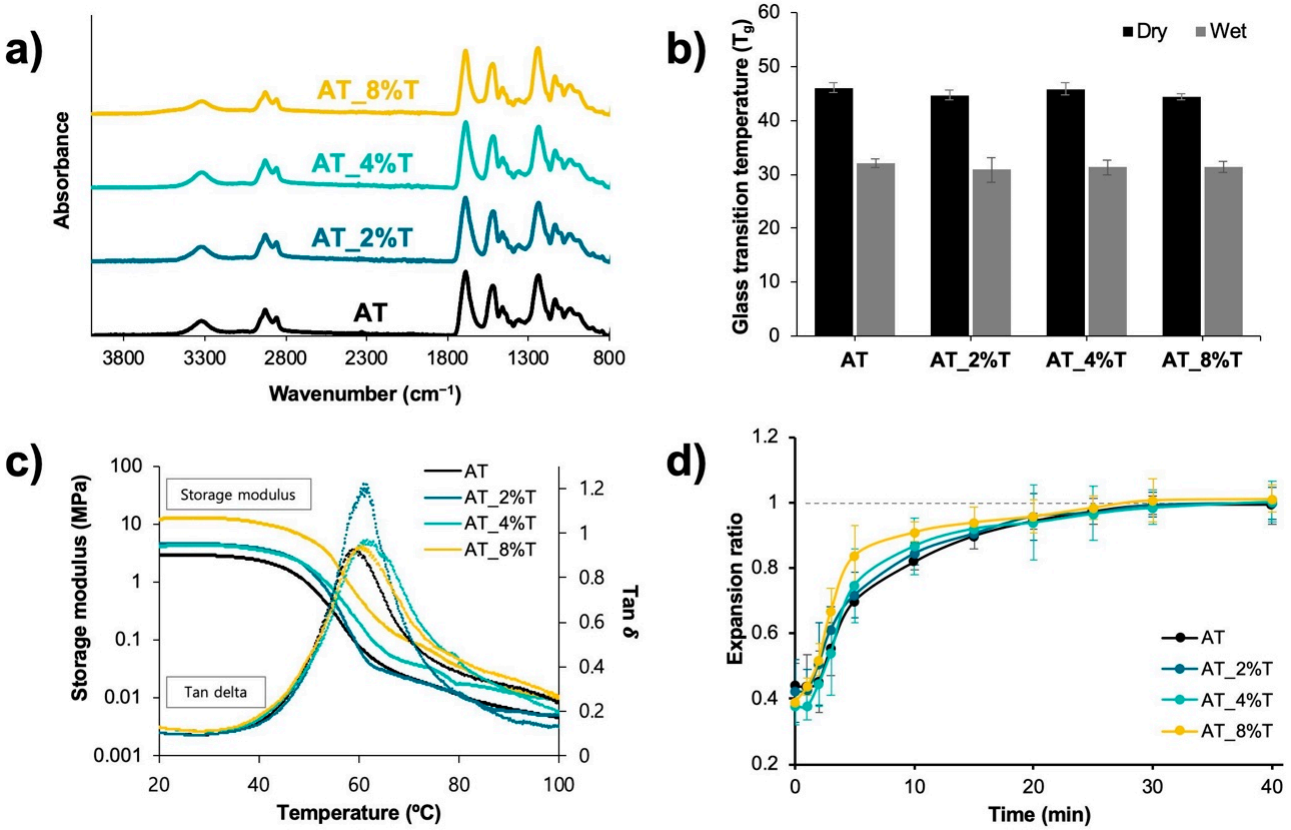

Figure 2. Chemical, thermal, and thermomechanical properties of ATIPA foams. (**a**) ATR-IR spectra of synthesized foams. (**b**) Dry and wet glass transition temperatures (T_gs) of each foam composition measured using DSC (n = 3). (**c**) Storage modulus and Tanδ measured as a function of temperature using DMA. (**d**) Expansion profile of crimped foam cylinders (2 mm diameter, 1.5 cm length) in 37 °C water (n = 3).

3.5. Thermomechanical Characterization

DMA was performed to analyze the mechanical properties of the foams as a function of temperature (Figure 2c). The T_g values of ATIPA foams measured by DMA (max tanδ) were all within the range of 59–62 °C which was comparable to the trend shown in DSC T_g values. Although the ATIPA foams had increasing storage modulus with the increasing tantalum content, their onsets of phase transition were all similar (46–49 °C), which indicates that the addition of tantalum microparticles does not alter the heat transferring rate of the material.

3.6. Expansion Study

Radially crimped cylindrical foams in the NED scale (2 mm diameter) were submerged in 37 °C water to characterize the shape memory effect (SME) of the foams (Figure 2d). Foams were crimped to a diameter of 0.64–0.77 mm for this study. The SME was quantified as 70%, 72%, 75%, and 84% shape recovery at the 5 min mark for AT, AT_2%T, AT_4%T, and AT_8%T, respectively. All of the foams showed over 99% shape recovery within 30 min at physiological conditions, indicating that the addition of tantalum microparticles does not impair the SME of the foams. The expansion rate was faster with the increase in tantalum content in the foams. Since the DMA results showed that the addition of tantalum does not have a significant effect on the heat transferring rate of the material, the faster expansion at AT_8%T foam is attributed to its higher crosslink density in the foam network due to the increased physical crosslinks. This result is consistent with previous work that showed SMP networks with higher crosslinking density recover faster to their original shapes than

the SMPs with a less dense network when both materials have similar glass transition properties [24].

3.7. Tensile Testing

The mechanical properties of the samples were characterized using tensile testing (Figure 3). The AT foams with the addition of 2% and 4% tantalum microparticles did not show any significant difference in the overall mechanical properties compared to AT foam. However, AT_8%T showed significantly higher Young's modulus, ultimate tensile strength, and significantly lower toughness and strain at break compared to other foam compositions. This indicates that high loading of tantalum particles (8%) results in stiffer and less tough foam matrix which could be attributed to the smaller pore sizes leading to higher crosslink density and tantalum particles replacing a higher portion of each polymer strut cross section.

a)

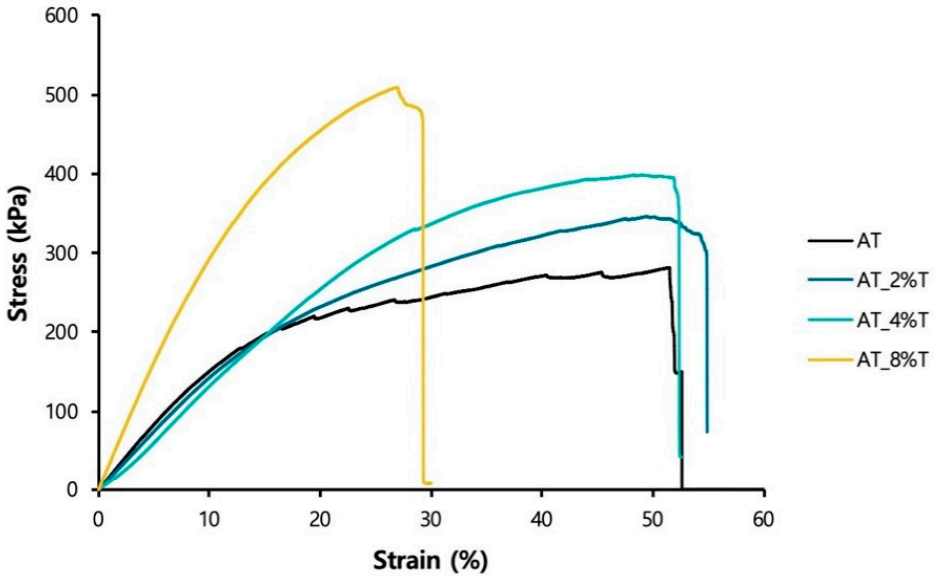

b)

	Ultimate tensile strength (kPa)	Toughness (kJ/m^3)	Strain at break (%)	Young's modulus (kPa)
AT	266 ± 54	110 ± 52	58 ± 17	1216 ± 287
AT_2%T	280 ± 86	147 ± 38	71 ± 17	1343 ± 571
AT_4%T	318 ± 78	151 ± 54	68 ± 16	1304 ± 226
AT_8%T	461 ± 38	84 ± 32	26 ± 9	3468 ± 801

Figure 3. Mechanical properties of ATIPA foams obtained from tensile testing. (**a**) Representative stress–strain curve for each foam composition. (**b**) Mechanical properties (ultimate tensile strength, toughness, strain at break, and Young's modulus) of ATIPA foams (n = 5).

3.8. X-ray Visibility Analysis

Foam samples were prepared with a thicknesses of 1, 2, 4, and 8 mm, as well as in neurovascular device prototypes (Figure 4a). X-ray images of the foams are shown in Figure 4b,c where a 0.5" aluminum plate is placed over samples in Figure 4c as a human skull analog. The numbers in Figure 4d represent 8 bit grayscale shift values relative to the image backgrounds. A minimum of 5 grayscale shift value is required in the visualization of the samples qualitatively. As tantalum microparticle loading % increased in AT foams,

the X-ray visibility was gradually improved. For AT foams, the sample with a thickness of 8 mm was lightly visible in Figure 4b (grayscale shift 6) but all thicknesses/types of AT samples were hardly visible with the skull analog. The addition of tantalum microparticles enabled visualization of ATIPA foams through aluminum plate, even at neurovascular device scales. The crimped device of AT_2%T foam was slightly visible (grayscale shift 5), which became more clearly visible in AT_4%T (grayscale shift 8) and AT_8%T (grayscale shift 12). Even the expanded device was visible in AT_4%T (grayscale shift 6) and AT_8%T (grayscale shift 8). This is a remarkable improvement compared to the previous study by Nash et al. where either crimped or expanded neurovascular device prototypes were barely visible through X-ray imaging (grayscale shift 2) [19].

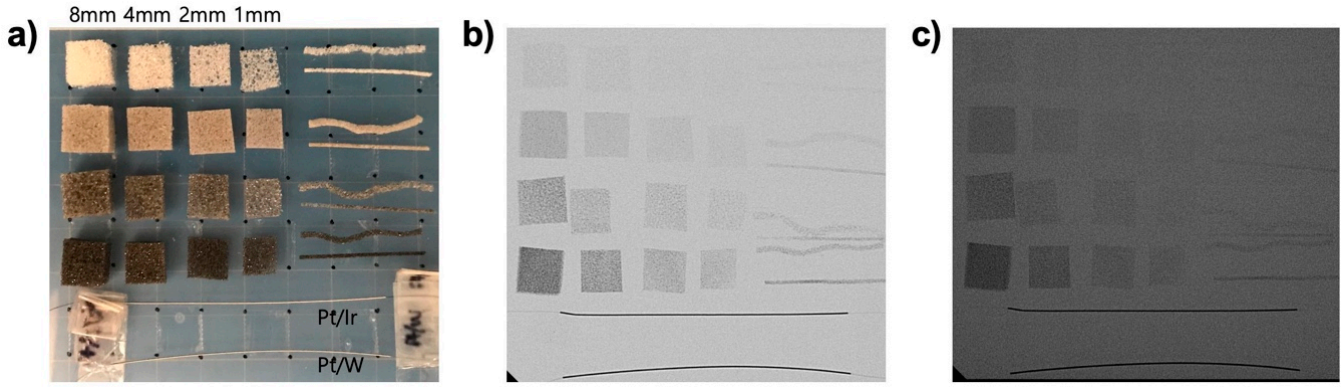

d)

	8mm	4mm	2mm	1mm	Expanded	Crimped
AT	**6** (2)	3 (1)	2 (1)	2 (0)	3 (0)	4 (2)
AT_2%T	**23** (**11**)	**11** (**5**)	**6** (3)	4 (1)	**7** (3)	**14** (**5**)
AT_4%T	**32** (**14**)	**14** (**8**)	**10** (**5**)	**6** (2)	**9** (**6**)	**19** (**8**)
AT_8%T	**71** (**27**)	**36** (**14**)	**20** (**9**)	**14** (**6**)	**19** (**8**)	**40** (**12**)
PT/Ir	**171** (**66**)					
PT/W	**176** (**68**)					

Figure 4. X-ray visibility of radiopaque ATIPA foams. (**a**) ATIPA foam samples with varying thicknesses and NED prototypes aligned on a plastic tray. The first row is AT foams with thicknesses of 8, 4, 2, and 1 mm. NED prototypes (cylinders with a diameter of 2 mm) in the expanded (top) and crimped (bottom) forms are at the right side of the image. The second, third, and fourth rows are AT_2%T, AT_4%T, and AT_8%T foams, respectively. For positive controls, 0.008″ OD 90/10 Pt/Ir coil and 0.008″ OD 92/8 Pt/W coil are used which are at the very bottom of the image. (**b**) Fluoroscopy image of the ATIPA foam samples. (**c**) Fluoroscopy image with an 0.5″ aluminum plate placed on top of the sample tray. (**d**) Mean grayscale shift values of samples from the background using ImageJ. Numbers without parentheses are from the image (**b**) and numbers with parentheses are from the image (**c**). Grayscale shift values 5 and above are bolded.

3.9. Cytocompatibility Test

The cytotoxicity of the ATIPA foams was investigated in vitro by adding foam extract media on the NIH/3T3 mouse fibroblasts. The cell viability was evaluated 48 h after adding the extract media using a resazurin assay. Figure 5 shows that the cell viabilities for each foam compositions were very high (>90%) which exceeds the 70% threshold to be considered non-cytotoxic. The cell viabilities for ATIPA samples did not show a significant difference from the negative control (100%). Furthermore, there was no significant difference found among the foam compositions.

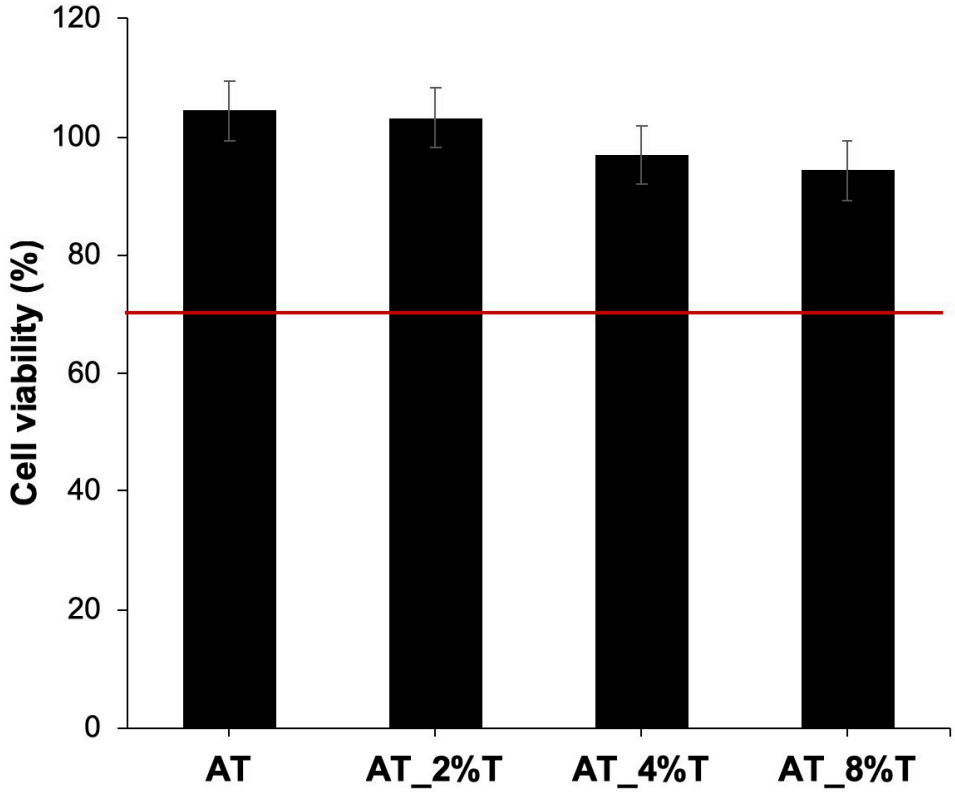

Figure 5. Cell viability results of the extract media test for the ATIPA foams (n = 3) 48 h after the addition of extraction media to NIH/3T3 cells. Cell viability above the red line (>70%) indicates that that there is no cytotoxic effect of extract media according to ISO 10993-5.

3.10. Effects of E-Beam Sterilization

AT and AT_4%T compositions were selected to analyze the E-beam sterilization effect on the ATIPA foams. E-beam irradiation can cause both cross-linking and scission of polymer bonds, depending on the polymer structure [25]. Chemical, thermal, shape recovery, and mechanical properties of the foams were compared before and after E-beam sterilization at 43.6 kGy (Figure 6). ATR-FTIR was performed to analyze the chemical properties of the foams (Figure 6a). The IR peaks of E-beam-sterilized foams were mostly not affected by the E-beam radiation except at 841 cm^{-1}, where a slight decrease in the peaks was observed in the E-beam-sterilized foams (Figure 6b). The absorption peak at 841 cm^{-1} is attributed to CH_2 rocking vibration [26,27]. The decrease in this peak indicates that crosslinking could have occurred in the polymer network. An electron beam can abstract hydrogen atoms from saturated carbon atoms forming macroradicals that could react with each other to form C-C crosslinks [28]. Glass transition temperatures were measured using DSC as shown in Figure 6c. The dry T_gs of E-beam-sterilized foams were significantly higher than non-treated foams. The dry T_gs of both AT and AT_4%T were increased approximately 4 °C after the E-beam treatment which could be a result of cross-linking of polymer structure. Wet T_gs and expansion profiles (Figure 6d) were not significantly different after the E-beam sterilization. Tensile testing results showed increased ultimate tensile strength, toughness, and strain at break for AT foams and increased toughness and strain at break for AT_4%T after E-beam irradiation which further supports that crosslinking occurred in the polymer system.

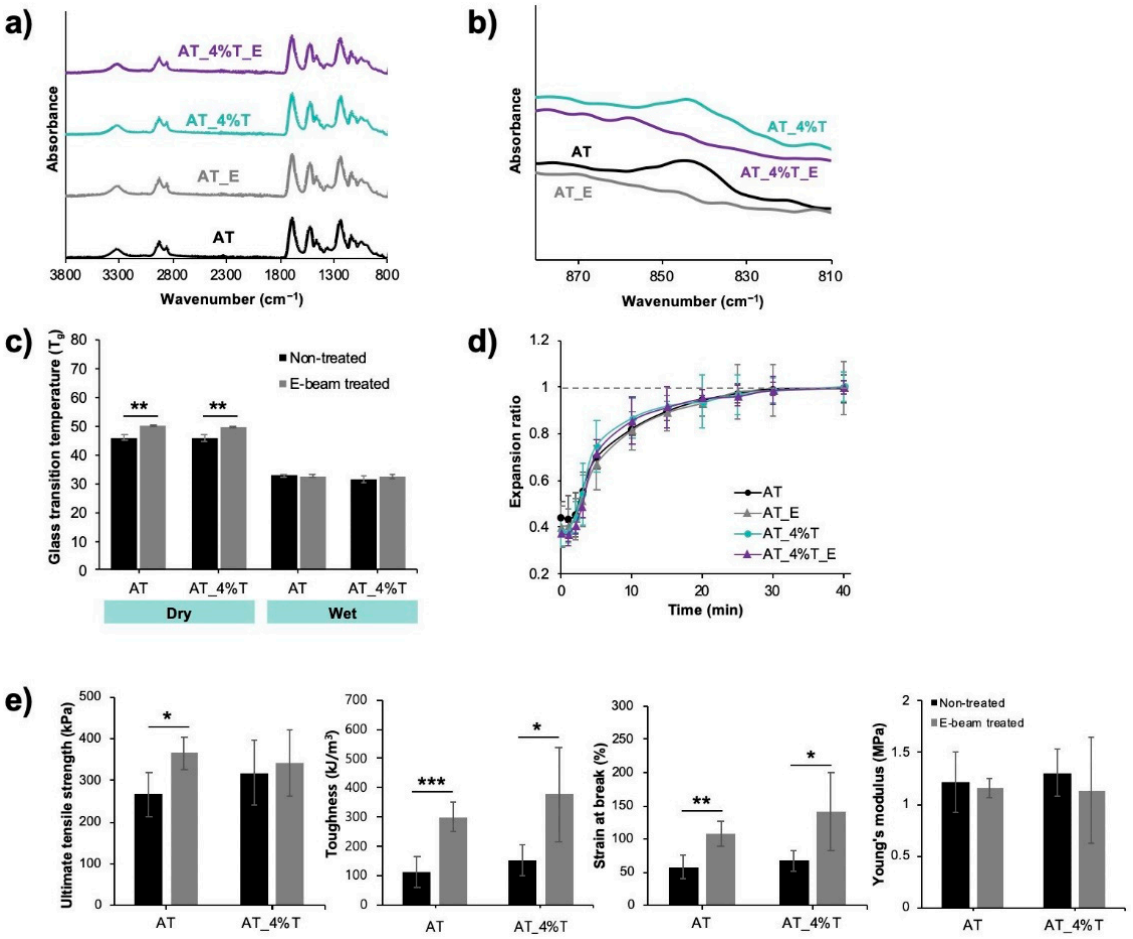

Figure 6. Electron-beam sterilization effect on AT and AT_4%T foams (* $p < 0.05$, ** $p < 0.01$, *** $p < 0.001$). (**a**) ATR-IR spectra for the range of 800–3800 cm^{-1} wavenumber. (**b**) Magnified ATR-IR spectra showing decreased peaks after E-beam. (**c**) Dry and wet T_gs measured using DSC (n = 3). (**d**) Expansion profile of crimped foams in 37 °C water (n = 3). (**e**) Tensile mechanical properties (n = 5).

3.11. In Vitro Degradation Study

The in vitro degradability of E-beam-sterilized ATIPA foams was analyzed in accelerated oxidative condition (20% H_2O_2, 37 °C) and in accelerated hydrolytic condition (0.1 N NaOH, 37 °C) over 90 days. Gravimetric analysis in Figure 7a shows that AT foam has 92.7% mass remaining after 90 days in the oxidative condition, which is not much different from its gel fraction (92.1%), indicating that oxidative degradation barely occurred in AT foams. As the tantalum content was increased in the foam, the mass loss over time was increased in the oxidative condition. H40 foam is one of the previously developed SMP foams from our group that contains tertiary amine bonds, which are oxidized to amine oxide and further form primary amines, carboxylic acids, and aldehydes [29]. The H40 foam was included in degradation studies to compare degradation profiles with those of ATIPA foams. When compared to H40, AT_T foams showed a steady mass loss, whereas H40 showed a sharp decrease at approximately 54 days. At 90 days, H40 had the lowest remaining mass of 24.6% followed by AT_8%T (27.6%), AT_4%T (44.5%), and AT_2%T (76.0%). In the hydrolytic degradation condition, ATIPA foams maintained a high percentage of their mass (84.4–89.1%, Figure 7b) at day 90. However, the remaining mass at day 90 were 6.2–8.4% lower than their gel fractions which suggests that hydrolytic degradation has occurred in the ATIPA foams. AT foams had the largest mass loss, which is expected due to their lowest gel fraction.

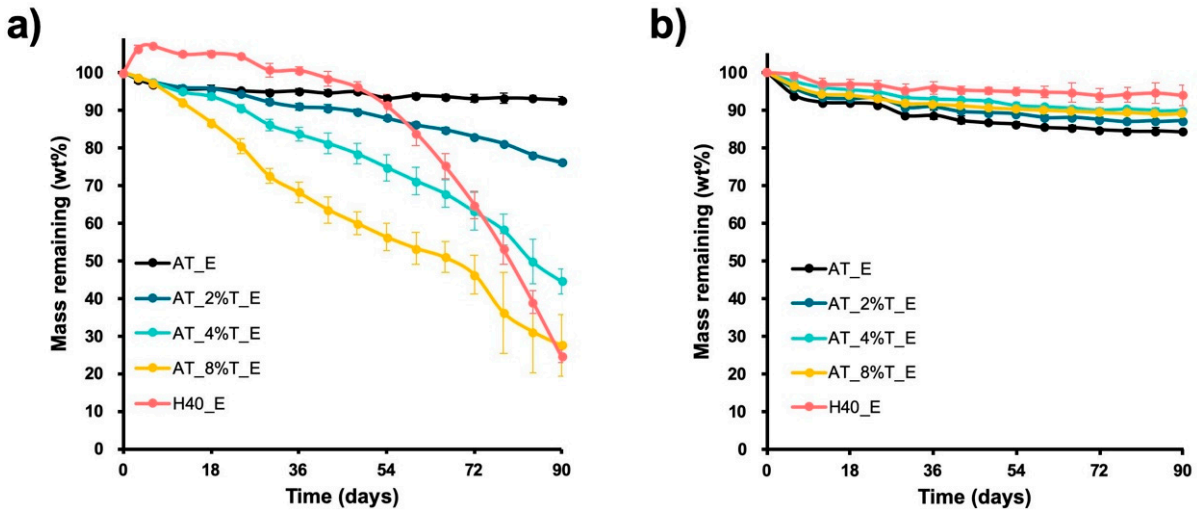

Figure 7. In vitro degradation studies performed by gravimetric analysis of ATIPA foams (n = 3) in (**a**) accelerated oxidative degradation solution (20% H_2O_2) and (**b**) accelerated hydrolytic degradation solution (0.1 N NaOH) at 37 °C over 90 days. H40 foam was used to compare ATIPA foams with the previously developed low-density SMP foam.

Morphological analysis was performed every 18 days on the degraded foams using SEM (Figure 8). In the oxidative degradation condition, AT and AT_2%T did not show a significant difference during 90 days (Figure 8a). AT_4%T started to show membrane degradation at day 54 and pore shrinkage and clustering were observed in day 72 and day 90. AT_8%T showed faster membrane degradation and pore shrinkage starting from day 36 which was followed by clustering in day 72 and total material collapse in day 90. In H40, membrane degradation was observed in day 18 followed by fragmentation of foam struts in day 54 and total material collapse in day 90. These morphological results were consistent with the gravimetric results, where H40 showed a sharp drop of mass at day 54, which is due to the strut fragmentation leading to a large loss of foam mass. In comparison, AT_4%T and AT_8%T foams did not show strut fragmentation like H40, but they showed foam clustering which led to their constant mass loss over time. In the hydrolytic degradation condition, all of the foam samples did not show a significant difference over 90 days (Figure 8b).

Chemical analysis of the degraded foams was performed every 18 days of degradation using ATR-FTIR (Figure 9). IR spectra of AT, AT_2%T, and AT_4%T did not change significantly throughout 90 days in the oxidative condition (Figure 9a) even though AT_2%T and AT_4%T had a quite significant mass loss of 23.9 and 55.5%, respectively, after 90 days of oxidative degradation. This indicates that the mass loss is attributed to tantalum dissolution, leading to the loss of mechanical stability of the foams. ATIPA foams with a higher content of tantalum have a lower portion of polymer in the foam struts and membrane. Thus, as the tantalum content increases, the mechanical stability of the foams decreases due to the dissolution of tantalum in the presence of H_2O_2 [30], and the physical fragmentation of polymer increases in the oxidative degradation condition. The overall decrease in the IR peaks in AT_8%T, which can be observed in Figure 9a, is likely due to the severe fragmentation and erosion of the polymer. In the hydrolytic degradation condition, all of the ATIPA foams showed an increase in the peak at 1597 cm^{-1} (N–H bend from primary amine) and decrease at 1182 and 1100 cm^{-1} (C–N stretch), which indicates that hydrolysis of amide bonds between ATIPA monomer and HDI has occurred (Figure 9b). The IR peaks of H40 foam in the oxidative condition (Figure 9a) demonstrate the scission of C–N bond from the tertiary amine as the peak at 1052 cm^{-1} (C–N stretch) decreases. The scission of C–N bond results in the formation of secondary amines and aldehydes which are further oxidized to form carboxylic acids. The carbonyl shift from 1689 to 1695 cm^{-1} indicates the formation of aldehydes and carboxylic acids. The peak at 1000 cm^{-1} corresponds to C–O stretch and the increase in the peak supports the formation

of carboxylic acids. The urea bonds (C=O) at 1638 cm^{-1} decreased over time as well as the amide II bonds at 1532 cm^{-1} and the amide III bonds at 1239 cm^{-1}. In the hydrolytic degradation condition, there were not any significant changes in the IR peaks during 90 days of H40 degradation. These degradation results of H40 are congruent with the previously reported degradation results of polyurethane SMP foams [29,31].

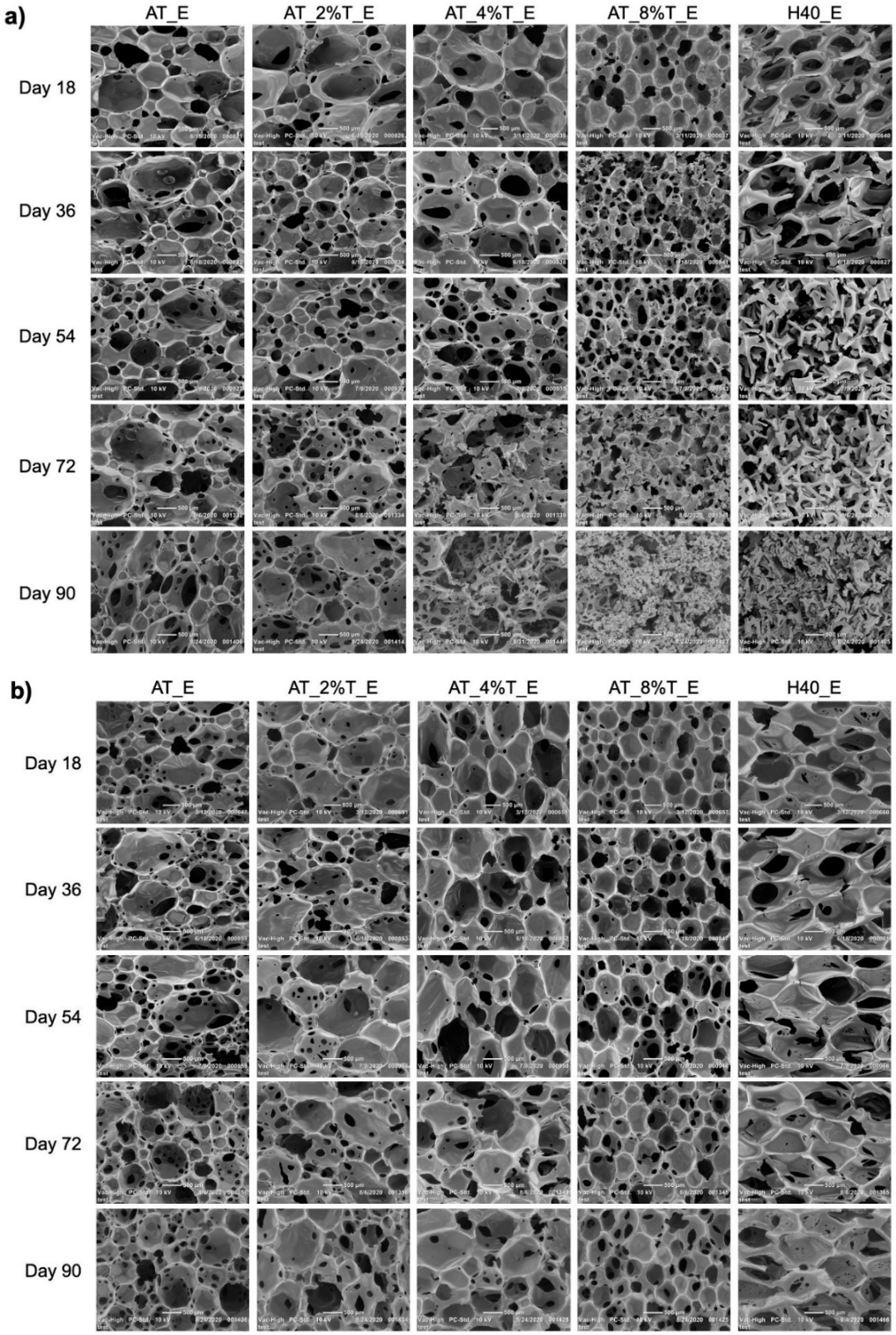

Figure 8. Morphological properties of degraded foams analyzed using SEM every 18 days up to 90 days. (**a**) The accelerated oxidative degradation condition. (**b**) The accelerated hydrolytic degradation condition.

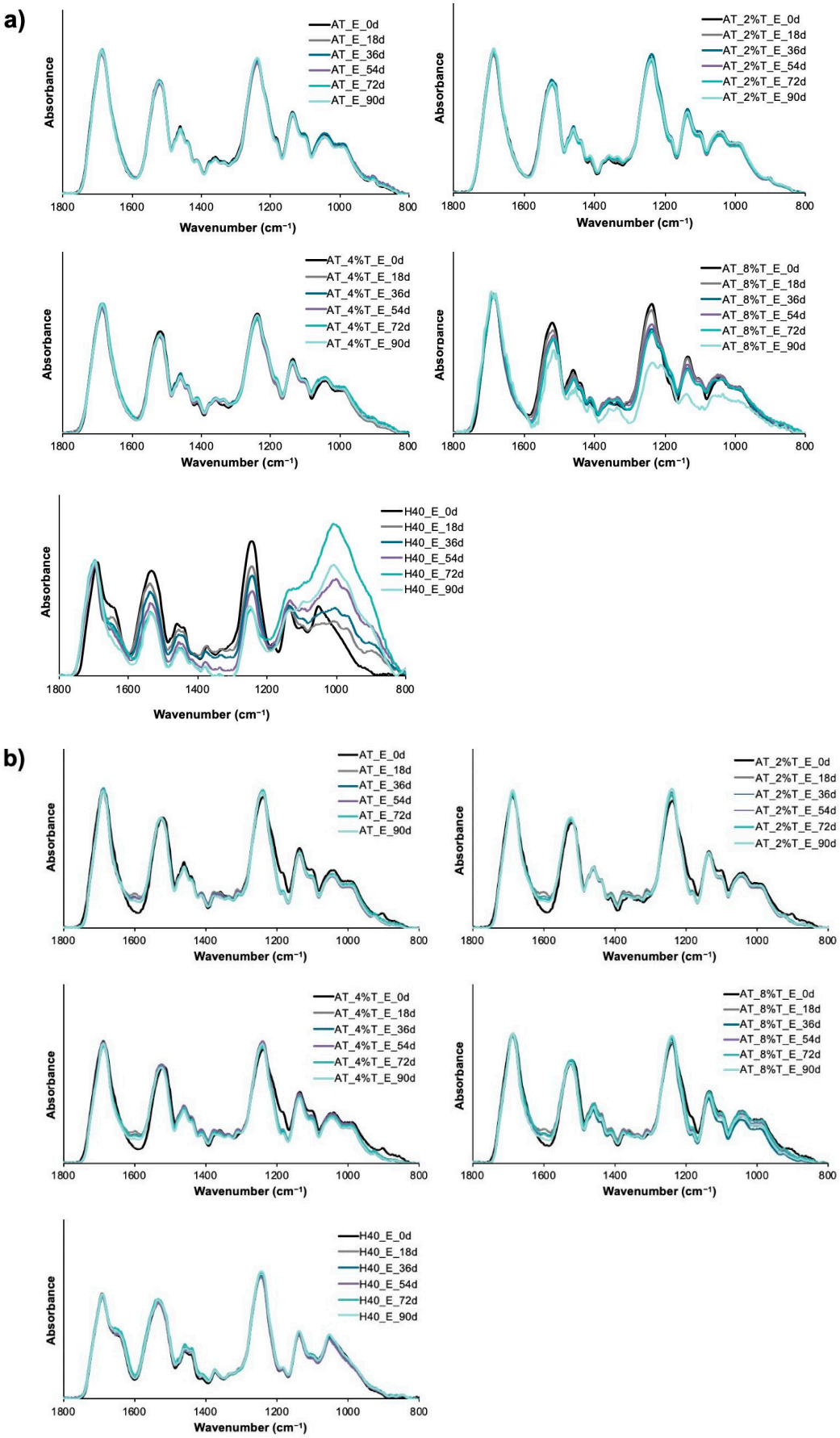

Figure 9. ATR-IR spectra of degraded foams over 90 days in (**a**) the accelerated oxidative degradation condition and (**b**) the accelerated hydrolytic degradation condition.

3.12. Extraction Study

ICP-OES was used to measure the amount of extracted tantalum from a AT_2%T neurovascular device (2 mm diameter, 1 cm length) in polar and non-polar extraction solutions (water and hexane, respectively) under exaggerated extraction conditions. The extracted tantalum from the device was below the detection limit (<0.1 μg/mL) in both polar and non-polar extraction solutions (Table 2).

Table 2. ICP-OES data for AT_2%T foams in various extraction solutions. (The detection limit is higher for 0.1 N NaOH due to additional dilution.)

Extraction Solution	Ta (μg/mL)	Ta (μg/Device)
Water	<0.1	<0.4
Hexane	<0.1	<0.4
20% H_2O_2	1.5 ± 2.3	6.7 ± 10.0
0.1 N NaOH	<0.2	<0.8

ICP-OES was also used to analyze tantalum extraction in degradation solutions (20% H_2O_2 and 0.1 N NaOH, 37 °C, 72 h) from AT_2%T neurovascular devices. An average of 1.5 ± 2.3 μg/mL tantalum was detected in 20% H_2O_2 and the total Ta amount extracted from the 1 cm neurovascular device was calculated to be 6.7 ± 10.0 μg/mL. Tantalum quantification was below the detection limit (<0.2 μg/mL) for the 0.1 N NaOH degradation solution.

4. Discussion

The goal of this study was to develop SMP foam compositions with appropriate X-ray visibility on the neurovascular scale. Previously developed ATIPA foams showed higher X-ray visibility with increasing density but showed limited visibility both in the crimped and expanded forms at the neurovascular scale [19]. Tantalum microparticles (~2 um) were added to ATIPA foam premix to combine the chemical approach of incorporating iodine motifs in the foam system and the physical approach of loading radio-dense tantalum microparticles to achieve sufficient X-ray visualization. In a clinical setting, a NED foam should be visible in its crimped shape through fluoroscopy to enable device visualization during delivery into an intracranial aneurysm. Once the delivered foam expands to fill the aneurysm sac, clinicians check whether the aneurysm is properly embolized or not by imaging a contrast agent introduced through the bloodstream (angiography). The expanded device should not be too highly radio-dense since it can block the visibility of the contrast agent flowing into the aneurysm that is not properly embolized, in which case more NED foams are delivered to pack the aneurysm. All of the fabricated AT_T foams (AT_2%T, AT_4%T, and AT_8%T) showed sufficient X-ray visibility in their crimped shape. However, AT_2%T and AT_4%T showed more desirable X-ray visibility in the expanded form, being less radiopaque than AT_8%T. Therefore, the optimal X-ray visibility could be achieved in the AT_2%T and AT_4%T foam compositions.

The tensile strength was increased with the increasing tantalum % in the foam, and the strain at break and toughness were decreased at a higher tantalum loading % (AT_8%T). This trend is consistent with Hasan et al.'s work, where the tungsten-loaded SMP foam's material stiffness and strength were increased up to 4 vol% tungsten and higher loading of the additives resulted in decreasing toughness and strain at break [18]. The tungsten-loaded SMP foams could achieve sufficient X-ray visibility at tungsten content greater than 6 vol%, of which the mechanical properties were diminished [18]. It is noteworthy that AT_2%T and AT_4%T foams showed sufficient X-ray visibility at the neurovascular scale with slightly improved mechanical properties. Further, ATIPA foams including AT_8%T have much higher toughness compared to previously developed low-density SMP foams due to the aromatic structures from the ATIPA monomer, which demonstrates that ATIPA foams can be mechanically stable under blood flow, lowering the risk of forming emboli due to foam fragmentation.

Biomedical devices can be sterilized in various ways, including ethylene oxide gas sterilization, E-beam radiation, and gamma radiation. E-beam radiation was chosen for a sterilization method in this study since E-beam radiation has more favorable sterilization conditions than the traditional ethylene oxide sterilization method (e.g., high heat, high humidity) for polyurethanes and also has shown to not prematurely actuate or alter any critical properties of SMP foam device in a previous study [32]. After E-beam sterilization, ultimate tensile strength (for AT foam only), toughness, and strain at break of ATIPA foams were increased but Young's modulus was not significantly impacted. Polymer crosslinking usually increases the modulus, ultimate tensile strength, and decreases the strain at break due to the crosslinking of intra- or intermolecular chains restricting the mobility of the polymer chains [28]. However, in highly porous material such as ATIPA foams, the modulus is not affected by the crosslinking of polymer chains [33]. The strain at break was increased after the E-beam radiation due to the elongation of pores to a higher extent resulting from the formation of tougher material after chain crosslinking.

In addition to the polymer chain crosslinking, E-beam sterilization changed the color of ATIPA foams to a more yellowish color (Figure S1a). The discoloration is commonly observed in various types of polymers after being irradiated by X-ray, gamma, or E-beam. The radiation can cause either permanent color change by rearranging bonds and forming covalent double bonds, or annealable color change by forming free radicals that are trapped in the polymeric matrix [28]. The discoloration observed in ATIPA foams was the latter, where the original color could be recovered after washing the material in water. The trapped free radicals can react with water molecules and anneal out the color center. After the recovery of the original color, radiopacity, T_g, and chemical properties of the ATIPA foams were analyzed. There was no significant difference in those properties after the washing step (Figure S1b–d), which indicates that the increase in T_g and change in the IR after E-beam radiation (Figure 6) are not relevant to the color center formation but are due to the chain crosslinking.

In the in vitro degradation studies, it should be noted that AT foams showed significantly improved biostability in the oxidative degradation condition compared to the previously developed low-density SMP foams (H40 in this study) due to the absence of the tertiary amine-containing monomers which are susceptible to oxidative degradation [29]. Therefore, the mass loss observed for AT_T foams over 90 days is due to the tantalum dissolution. However, the mass loss over 90 days (24, 55, and 72 wt% for AT_2%T, AT_4%T, and AT_8%T, respectively) was larger than the tantalum wt% in the foams (22, 36, and 52 wt%) and the mass consistently decreased during 90 days. This indicates that the mass loss is also associated with the loss of foam particulates, as the foam structure becomes weaker during the tantalum dissolution. Since fragments from neurovascular foam possess the possibility of generating emboli in the bloodstream, the more oxidatively biostable AT_2%T is more appropriate composition for neurovascular devices than AT_4%T. However, it is very unlikely for the degrading material to enter the circulation since the developing clot isolates the foam material a few hours after the device implantation, and the foam is trapped in thrombus and developing scar tissue.

Extraction studies showed that tantalum was extracted out of the AT_2%T device only in 20% H_2O_2, but not in water, hexane, or 0.1 N NaOH extraction solutions. This is attributed to the higher solubility of tantalum in the H_2O_2 solution compared to other extraction solutions, which supports our degradation study results [30]. However, the extracted amounts were still very small, which did not exceed 20 μg per neurovascular device over three days in the accelerated condition. For a large aneurysm with a diameter of 25 mm, 234 cm of foam devices is needed to achieve a packing density of 90%, which is a high-end estimation for the amount of implanted foams. In this case, 0.031 mg/kg tantalum will be extracted per day for a 50 kg adult, which is five orders of magnitude lower than the LD50 (lethal dose) level of tantalum (8000 mg/kg) [34]. The extraction study results along with the cell viability results ensure the biocompatibility of the AT_2%T device even with a much longer length of the foam device.

One limitation of AT_T foams is the short working time (~2 min), as shown in the expansion profile (Figure 2d). Clinicians require a working time of approximately 5–10 min, which is a time to deliver the crimped foam through the blood vessel into the aneurysm sac using a microcatheter. Several methods can increase the working time of AT_T foams. First, more hydrophobic monomers could be used in the foam synthesis to decrease the water penetration rate into the crimped foam. Second, the foams can be crimped to a smaller diameter, which would decrease the water penetration rate as well. In order to crimp foams more tightly, foams with a lower density could be fabricated by increasing the amount of blowing agent or using different surfactants. The foams can also be mechanically crimped into a smaller diameter since the foams could only be crimped down to a diameter of 0.6 mm in this study due to the crimper used, which had a minimum crimping diameter of 0.6 mm. Therefore, a crimper that has a smaller minimum crimping diameter can decrease the crimped diameter of the AT_T foams. For feasible delivery of the foam device into a tortuous human neurovasculature, the use of 0.017″ (0.43 mm) or smaller inner diameter (ID) catheter is required. Thus, the foams would need to be crimped to a smaller diameter than 0.43 mm to be used for a neurovascular embolization device. In addition to increasing the working time and decreasing the crimped diameter, the biocompatibility of the degraded products needs to be analyzed in vitro and in vivo for future work to ensure the safety of using AT_T foams in neurovascular embolization applications.

5. Conclusions

The radiopacity of SMP foams was improved by adding 2, 4, and 8 vol% tantalum microparticles to triiodobenzene-containing SMP foams (ATIPA foams). The fabricated ATIPA foam-tantalum composites (AT_T) demonstrated clinically relevant thermal properties, good mechanical properties, and excellent cytocompatibilities. ATIPA foams with a higher tantalum loading % showed faster shape recovery, increased X-ray visibility, and faster oxidative degradation. AT_2%T was considered to be the optimal foam composition to be used as a neurovascular embolization device due to its optimal radiopacity in a clinical setting and high oxidative stability compared to other AT_T foams. The radiopaque SMP foams developed in this study show great promise for use in neurovascular embolization applications.

Supplementary Materials: The following are available online at https://www.mdpi.com/2504-477X/5/1/14/s1, Figure S1: Effect of E-beam sterilization and washing with water on AT and AT_4%T foams.

Author Contributions: Conceptualization, L.K.J., L.D.N. and D.J.M.; methodology, L.K.J., L.D.N., G.K.F., and D.J.M.; software, L.K.J.; validation, L.K.J., L.D.N. and D.J.M.; formal analysis, L.K.J.; investigation, L.K.J.; resources, L.K.J.; data curation, L.K.J., G.K.F., T.C., and A.S.; writing—original draft preparation, L.K.J.; writing—review and editing, L.D.N., G.K.F., A.S., and D.J.M.; visualization, L.K.J.; supervision, D.J.M.; project administration, D.J.M.; funding acquisition, D.J.M. All authors have read and agreed to the published version of the manuscript.

Funding: This work was supported by the NIH National Institute of Neurological Disorders and Stroke, grant number U01-NS089692.

Institutional Review Board Statement: Not applicable.

Informed Consent Statement: Not applicable.

Data Availability Statement: The data presented in this study are openly available at https://doi.org/10.18738/T8/A4JFTJ.

Acknowledgments: The authors would like to acknowledge Lance Graul for his technical support in tensile testing, Sam Briggs for his technical support in DMA, and Tyler Touchet for his assistance in DMA and the X-ray imaging. The authors would like to thank the Legend Technical Services Inc. for their ICP-OES analysis and Bryan Tomlin for his suggestions in the elemental analysis.

Conflicts of Interest: Shape Memory Medical Inc. (SMM) owns the commercial license for the SMP foam material described in this work. The authors disclose that D.J.M. is a Director and Chief Technology Officer at SMM and holds stock. L.D.N. is currently employed by SMM and holds stock. SMM did not fund this work.

References

1. Keedy, A. An overview of intracranial aneurysms. *McGill J. Med. MJM Int. Forum Adv. Med. Sci. Stud.* **2006**, *9*, 141–146.
2. Bonneville, F.; Sourour, N.; Biondi, A. Intracranial Aneurysms: An Overview. *Neuroimaging Clin.* **2006**, *16*, 371–382. [CrossRef] [PubMed]
3. Wardlaw, J.M.; White, P.M. The detection and management of unruptured intracranial aneurysms. *Brain* **2000**, *123*, 205–221. [CrossRef] [PubMed]
4. Hop, J.W.; Rinkel, G.J.; Algra, A.; van Gijn, J. Case-fatality rates and functional outcome after subarachnoid hemorrhage: A systematic review. *Stroke* **1997**, *28*, 660–664. [CrossRef] [PubMed]
5. Hong, Y.; Wang, Y.-J.; Deng, Z.; Wu, Q.; Zhang, J.-M. Stent-assisted coiling versus coiling in treatment of intracranial aneurysm: A systematic review and meta-analysis. *PLoS ONE* **2014**, *9*, e82311. [CrossRef]
6. Pierot, L.; Cognard, C.; Anxionnat, R.; Ricolfi, F. Endovascular treatment of ruptured intracranial aneurysms: Factors affecting midterm quality anatomic results: Analysis in a prospective, multicenter series of patients (CLARITY). *Am. J. Neuroradiol.* **2012**, *33*, 1475–1480. [CrossRef]
7. Gonzalez, N.R.; Duckwiler, G.; Jahan, R.; Murayama, Y.; Viñuela, F. Challenges in the endovascular treatment of giant intracranial aneurysms. *Neurosurgery* **2006**, *59*, S3-113–S3-124. [CrossRef]
8. Kwan, E.S.; Heilman, C.B.; Shucart, W.A.; Klucznik, R.P. Enlargement of basilar artery aneurysms following balloon occlusion—"water-hammer effect": Report of two cases. *J. Neurosurg.* **1991**, *75*, 963–968. [CrossRef] [PubMed]
9. Sluzewski, M.; van Rooij, W.J.; Slob, M.J.; Bescós, J.O.; Slump, C.H.; Wijnalda, D. Relation between aneurysm volume, packing, and compaction in 145 cerebral aneurysms treated with coils. *Radiology* **2004**, *231*, 653–658. [CrossRef] [PubMed]
10. Singhal, P.; Rodriguez, J.N.; Small, W.; Eagleston, S.; Van de Water, J.; Maitland, D.J.; Wilson, T.S. Ultra low density and highly crosslinked biocompatible shape memory polyurethane foams. *J. Polym. Sci. Part B Polym. Phys.* **2012**, *50*, 724–737. [CrossRef] [PubMed]
11. Herting, S.M.; Ding, Y.; Boyle, A.J.; Dai, D.; Nash, L.D.; Asnafi, S.; Jakaitis, D.R.; Johnson, C.R.; Graul, L.M.; Yeh, C.; et al. In vivo comparison of shape memory polymer foam-coated and bare metal coils for aneurysm occlusion in the rabbit elastase model. *J. Biomed. Mater. Res. B Appl. Biomater.* **2019**, *107*, 2466–2475. [CrossRef] [PubMed]
12. Boyle, A.J.; Wierzbicki, M.A.; Herting, S.; Weems, A.C.; Nathan, A.; Hwang, W.; Maitland, D.J. In vitro performance of a shape memory polymer foam-coated coil embolization device. *Med. Eng. Phys.* **2017**, *49*, 56–62. [CrossRef] [PubMed]
13. Boyle, A.J.; Landsman, T.L.; Wierzbicki, M.A.; Nash, L.D.; Hwang, W.; Miller, M.W.; Tuzun, E.; Hasan, S.M.; Maitland, D.J. In vitro and in vivo evaluation of a shape memory polymer foam-over-wire embolization device delivered in saccular aneurysm models. *J. Biomed. Mater. Res. B Appl. Biomater.* **2016**, *104*, 1407–1415. [CrossRef] [PubMed]
14. Rodriguez, J.N.; Clubb, F.J.; Wilson, T.S.; Miller, M.W.; Fossum, T.W.; Hartman, J.; Tuzun, E.; Singhal, P.; Maitland, D.J. In vivo response to an implanted shape memory polyurethane foam in a porcine aneurysm model. *J. Biomed. Mater. Res. A* **2014**, *102*, 1231–1242. [CrossRef] [PubMed]
15. Horn, J.; Hwang, W.; Jessen, S.L.; Keller, B.K.; Miller, M.W.; Tuzun, E.; Hartman, J.; Clubb, F.J., Jr.; Maitland, D.J. Comparison of shape memory polymer foam versus bare metal coil treatments in an in vivo porcine sidewall aneurysm model. *J. Biomed. Mater. Res. B Appl. Biomater.* **2017**, *105*, 1892–1905. [CrossRef] [PubMed]
16. Jansen, A.-J.S.; van Schaik, P.M.; Martens, J.M.; Reijnen, M.M.P.J. Embolization of the false lumen using IMPEDE-FX embolization plugs as part of treatment of an infrarenal post-dissection aneurysm: A case report. *CVIR Endovasc.* **2020**, *3*, 91. [CrossRef] [PubMed]
17. Kashyap, D.; Kishore Kumar, P.; Kanagaraj, S. 4D printed porous radiopaque shape memory polyurethane for endovascular embolization. *Addit. Manuf.* **2018**, *24*, 687–695. [CrossRef]
18. Hasan, S.M.; Harmon, G.; Zhou, F.; Raymond, J.E.; Gustafson, T.P.; Wilson, T.S.; Maitland, D.J. Tungsten-loaded SMP foam nanocomposites with inherent radiopacity and tunable thermo-mechanical properties. *Polym. Adv. Technol.* **2016**, *27*, 195–203. [CrossRef]
19. Nash, L.; Browning Monroe, M.; Ding, Y.-H.; Ezell, K.; Boyle, A.; Kadirvel, R.; Kallmes, D.; Maitland, D. Increased X-ray Visualization of Shape Memory Polymer Foams by Chemical Incorporation of Iodine Motifs. *Polymers* **2017**, *9*, 381. [CrossRef]
20. Balla, V.K.; Bose, S.; Davies, N.M.; Bandyopadhyay, A. Tantalum—A bioactive metal for implants. *JOM* **2010**, *62*, 61–64. [CrossRef]
21. Cristea, D.; Ghiuta, I.; Munteanu, D. Tantalum based materials for implants and prostheses applications. *Bull. Transilv. Univ. Brasov Eng. Sci. Ser. I* **2015**, *8*, 151.
22. Balla, V.K.; Banerjee, S.; Bose, S.; Bandyopadhyay, A. Direct laser processing of a tantalum coating on titanium for bone replacement structures. *Acta Biomater.* **2010**, *6*, 2329–2334. [CrossRef] [PubMed]
23. Ionita, C.N.; Loughran, B.; Jain, A.; Vasan, S.S.; Bednarek, D.R.; Levy, E.; Siddiqui, A.H.; Snyder, K.V.; Hopkins, L.; Rudin, S. *New Head Equivalent Phantom for Task and Image Performance Evaluation Representative for Neurovascular Procedures Occurring in the Circle of Willis*; International Society for Optics and Photonics: San Diego, CA, USA, 2012; Volume 8313, p. 83130Q.

24. Yakacki, C.M.; Shandas, R.; Lanning, C.; Rech, B.; Eckstein, A.; Gall, K. Unconstrained recovery characterization of shape-memory polymer networks for cardiovascular applications. *Biomaterials* **2007**, *28*, 2255–2263. [CrossRef] [PubMed]
25. Lee, E.H.; Rao, G.R.; Mansur, L.K. LET effect on cross-linking and scission mechanisms of PMMA during irradiation. *Radiat. Phys. Chem.* **1999**, *55*, 293–305. [CrossRef]
26. Haris, M.; Kathiresan, S.; Mohan, S. FT-IR and FT-Raman spectra and normal coordinate analysis of poly methyl methacrylate. *Pharma Chem.* **2010**, *2*, 316–323.
27. Nallasamy, P.; Anbarasan, P.; Mohan, S. Vibrational spectra and assignments of cis-and trans-1, 4-polybutadiene. *Turk. J. Chem.* **2002**, *26*, 105–112.
28. Ramachandran, P.; Naskar, K.; Nando, G.B. Effect of electron beam irradiation on the structure–property relationship of ethylene octene copolymer and polydimethyl siloxane rubber blends. *Rubber Chem. Technol.* **2016**, *89*, 477–498. [CrossRef]
29. Weems, A.C.; Wacker, K.T.; Carrow, J.K.; Boyle, A.J.; Maitland, D.J. Shape memory polyurethanes with oxidation-induced degradation: In vivo and in vitro correlations for endovascular material applications. *Acta Biomater.* **2017**, *59*, 33–44. [CrossRef]
30. Kuiry, S.; Seal, S.; Fei, W.; Ramsdell, J.; Desai, V.; Li, Y.; Babu, S.; Wood, B. Effect of pH and H_2O_2 on Ta Chemical Mechanical Planarization: Electrochemistry and X-ray Photoelectron Spectroscopy Studies. *J. Electrochem. Soc.* **2002**, *150*, C36. [CrossRef]
31. Jang, L.K.; Fletcher, G.K.; Monroe, M.B.B.; Maitland, D.J. Biodegradable shape memory polymer foams with appropriate thermal properties for hemostatic applications. *J. Biomed. Mater. Res. A* **2020**, *108*, 1281–1294. [CrossRef]
32. Muschalek, R.; Nash, L.; Jones, R.; Hasan, S.M.; Keller, B.K.; Monroe, M.B.B.; Maitland, D.J. Effects of sterilization on shape memory polyurethane embolic foam devices. *J. Med. Devices* **2017**, *11*, 031011. [CrossRef] [PubMed]
33. Oláh, L.; Filipczak, K.; Czvikovszky, T.; Czigány, T.; Borbás, L. Changes of porous poly (ε-caprolactone) bone grafts resulted from e-beam sterilization process. *Radiat. Phys. Chem.* **2007**, *76*, 1430–1434. [CrossRef]
34. Coulston, F.; Korte, F. Heavy metal toxicity, safety and hormology. *Environ. Qual. Saf. Suppl.* **1975**, *1*, 1–120.